2015/01/20
Head Id: 271760
Archive Id: 274430
Archive Date: 2014/12/15
Archive Tag: trunk

Search for SUSY using razor variables in events with b-tagged jets in pp collisions at $\sqrt{s} = 8$ TeV

The CMS Collaboration

Abstract

An inclusive search for supersymmetry in events with at least one bottom-quark jet is carried out on proton-proton collision data collected by the CMS experiment in 2012 at a center-of-mass energy of 8 TeV. The dataset size corresponds to an integrated luminosity of 19.3 fb^{-1}. The two-dimensional event distribution for the razor variables R^2 and M_R is studied in events with and without leptons. The data are consistent with the expected background, modeled by an empirical function. Exclusion limits on the supersymmetric particle masses at a 95% confidence level are derived in several simplified supersymmetric scenarios for several choices of the branching fractions. By combining the likelihoods of the razor search in events without leptons and an exclusive single-lepton search, an improved bound on the top-squark mass is obtained. Assuming the lightest supersymmetric particle mass is 100 GeV, the branching fraction dependent (independent) pair production of gluinos and top squarks is excluded for gluino masses up to 1310 (1175) GeV and for top-squark masses up to 730 (645) GeV.

1 Introduction

Supersymmetry (SUSY) is a proposed symmetry of nature, which introduces a bosonic partner for every fermion and vice versa [1–9]. Supersymmetric extensions of the standard model (SM) that include a stable new particle at the electroweak scale are well-motivated because they may explain the origin of the dark matter and allow for the grand unification of strong and electroweak forces. The discovery of the Higgs boson [10–12] at the Large Hadron Collider (LHC) has renewed interest in "natural" SUSY models, which minimize the fine-tuning associated with the observed value of the Higgs boson mass and its radiative corrections in the SM. In the typical spectrum of these models, the lightest neutralino and chargino are the lightest (LSP) and next-to-lightest (NLSP) SUSY particles, respectively. The bottom and top squarks are the lightest squarks, and the gluino is heavier than these particles but potentially accessible at the LHC [13]. Events are characterized by an abundance of jets originating from the hadronization of bottom quarks, a feature that we exploit in this study. Previous searches for natural SUSY by the Compact Muon Solenoid (CMS) [14–17] and ATLAS Collaborations [18–22] at a center-of-mass energy of $\sqrt{s} = 8$ TeV have excluded gluino masses up to 1.3 TeV and squark masses up to 700 GeV, for fixed choices of the decay modes of the produced SUSY partners.

We present an inclusive search for squarks and gluinos in the context of natural SUSY [13]. Natural SUSY spectra consist of a gluino, the lightest 3rd generation squarks, and a charged and a neutral higgsino. This is the minimal particle content needed in SUSY theories to stabilize the Higgs mass. Within the domain of natural SUSY scenarios, several simplified models [23–27] are considered (see Sec. 2), defined by a specific production mechanism of SUSY particle pairs, considering at most two decay modes at the same time.

The search is performed on events with two or more jets, at least one of which is identified as originating from a bottom quark (jet b tagging). The search is carried out on the data collected by the CMS Collaboration in proton-proton collisions at $\sqrt{s} = 8$ TeV in 2012, corresponding to an integrated luminosity of 19.3 fb^{-1}. We exploit the difference in the shapes of the distributions in the razor variables R^2 and M_R [28, 29] to distinguish the signal from the SM background.

The razor variables M_R and R^2 describe the two-jet topology resulting from the production of two squarks, each decaying to a quark and the LSP, assumed to be a stable neutralino $\widetilde{\chi}_1^0$. The four-momenta of the two jets are used to compute M_R and M_T^R, defined as

$$M_R \equiv \sqrt{(|\vec{p}^{\,j_1}| + |\vec{p}^{\,j_2}|)^2 - (p_z^{j_1} + p_z^{j_2})^2}\,, \tag{1}$$

$$M_T^R \equiv \sqrt{\frac{E_T^{miss}(p_T^{j_1} + p_T^{j_2}) - \vec{E}_T^{miss}\cdot(\vec{p}_T^{\,j_1} + \vec{p}_T^{\,j_2})}{2}}\,, \tag{2}$$

where $\vec{p}_{j_i}$, $\vec{p}_T^{\,j_i}$, and $p_z^{j_i}$ are the momenta of the i_{th}-jet, its transverse and longitudinal components, respectively, while E_T^{miss} and p_{Ti}^{j} are the magnitude of $\vec{E}_T^{miss}$ and $\vec{p}_T^{\,j_i}$, respectively. While M_T^R quantifies the transverse momentum imbalance, while M_R estimates the energy scale in the event. The razor dimensionless ratio is defined as

$$R \equiv \frac{M_T^R}{M_R}\,. \tag{3}$$

In this search, each event is reduced to a two-jet topology by clustering the selected particles (jets and leptons) into two "megajets" [29–31]. The megajets are defined by dividing the selected particles of each event into two groups. All the possible pairs of groups with at least one particle per group are considered. The sum of the four-momenta of the particles in a given

group is the megajet four-momentum. When more than two particles are reconstructed, several megajet assignments are possible. In this analysis we consider the assignment that minimizes the sum of the invariant masses of the two megajets.

The analysis is performed on several exclusive datasets (referred to as *razor boxes*), differing in the lepton and jet multiplicity. Each box with fewer than two identified leptons is analyzed in exclusive b-tagged jet multiplicity bins in order to maximize the sensitivity to both direct and cascade production of third generation squarks. For a given box and b-tagged jet multiplicity, the background shape is modeled in two rectangular regions of the (M_R, R^2) plane (sidebands), designed so that bias induced on shape determination by any possible signal contamination is negligible. The background shape is then extrapolated to the rest of the (M_R, R^2) plane (signal-sensitive region) to estimate the SM background contribution. We observe good agreement between the predicted background and the data yields in the signal-sensitive regions. This result is then interpreted in the context of several SUSY simplified models by performing by performing a hypothesis test between the background-only and signal-plus-background hypotheses using simultaneously the data in the two sidebands and the signal-sensitive region [32].

This search extends the previous search performed with the CMS experiment using the same analysis technique on the data collected at a center-of-mass energy of 7 TeV [30, 31]. The razor variables have also been used by the ATLAS Collaboration for a multi-channel search for SUSY at a center-of-mass energy of 7 TeV [33].

In addition, we obtain an improved bound on the top-squark pair production, with respect to the previous CMS results, by combining the all-hadronic razor boxes with a dedicated exclusive top-squark search in events with one lepton [14]. The exclusive single-lepton search contribues to the combination through the event category with the lowest expected cross section upper limit, for a given value of the top squark and LSP mass. In this combination, only the razor hadronic boxes are considered. An explicit lepton veto is applied so that the results of the two searches are mutually exclusive. As neither search observes an excess above the estimated background, the results are interpreted here as limits on colored sparticle production cross sections. Details on the exclusive top-squark search can be found in Ref. [14].

This paper is organized as follows. Section 2 describes the spectra of the simplified natural SUSY models targeted by this study. The CMS detector is briefly described in Section 3. The event selection and razor variables are described in Sections 4 and 5, respectively. The statistical model used to describe the SM backgrounds as well as the comparisons between predicted and observed yields in the search regions are detailed in Section 6, followed by a summary of the limit setting procedure in Section 7. The interpretation of the results in terms of simplified natural SUSY models and the conclusions are then presented in Sections 8 and 9, respectively.

2 Simplified natural SUSY models

For this set of interpretations, a simplified natural SUSY spectrum [13] is taken as a reference. The LSP is assumed to be a neutralino $\widetilde{\chi}_1^0$, 5 GeV lighter than a chargino $\widetilde{\chi}_1^\pm$. The chargino is forced to be the NLSP, with 100% branching fraction for the decay involving a virtual W (W^*), $\widetilde{\chi}_1^\pm \to W^* \widetilde{\chi}_1^0$. Three other SUSY partners are assumed to be accessible at the LHC, namely the gluino and the lightest top and bottom squarks. The rest of the SUSY spectrum is assumed to be decoupled, with masses large enough to be inaccessible at the LHC. The SUSY partners composing this natural SUSY spectrum are summarized in Fig. 1, together with the possible decay modes.

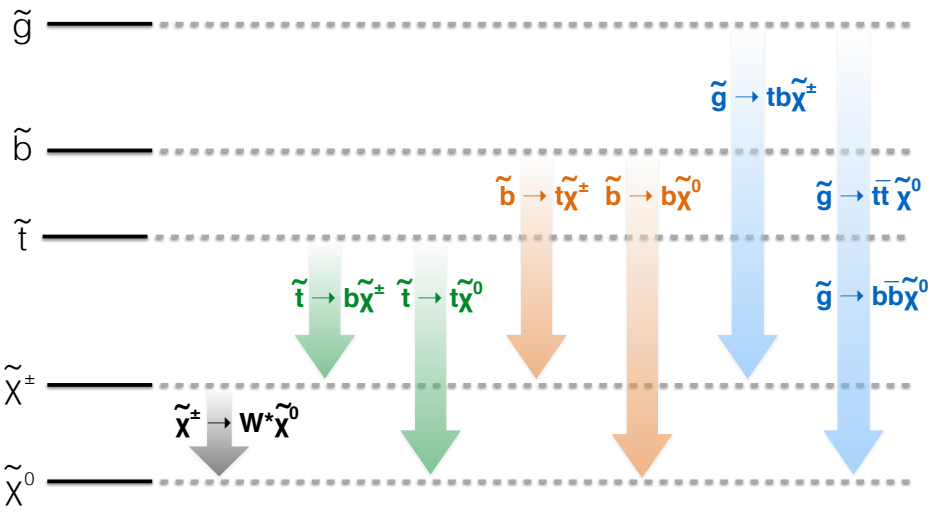

Figure 1: Simplified natural SUSY spectrum considered as a benchmark for result interpretations. The neutralino is forced to be the lightest SUSY particle. The difference in mass between the chargino and the neutralino is fixed at 5 GeV. Gluino and same-flavor squark pair production are considered in separate models, scanning the masses of the produced SUSY particle and the neutralino.

In the context of this natural spectrum, five simplified models [23–27] are considered for gluino pair production, based on three-body gluino decays [34]:

- **T1bbbb**: pair-produced gluinos, each decaying with a 100% branching fraction to a pair of bottom quarks and the LSP.
- **T1tbbb**: pair-produced gluinos, each decaying with a 50% branching fraction to a pair of bottom quarks and the LSP or a top quark, a bottom quark, and the NLSP.
- **T1ttbb**: pair-produced gluinos, each decaying with a 50% branching fraction to a pair of bottom quarks and the LSP or a pair of top quarks and the LSP.
- **T1tttb**: pair-produced gluinos, each decaying with a 50% branching fraction to a pair of top quarks and the LSP or a top quark, a bottom quark, and the NLSP.
- **T1tttt**: pair-produced gluinos, each decaying with a 100% branching fraction to a pair of top quarks and the LSP.

The corresponding Feynman diagrams are shown in Fig. 2. Similar models were not considered, for which the same final states are obtained from two-body gluino decays to squark and quark and the consequent cascade.

In addition, the following three simplified models are considered for the production of top-squark pairs:

- **T2bW***: pair-produced top squarks, each decaying with a 100% branching fraction to a bottom quark and the NLSP.
- **T2tb**: pair-produced top squarks, each decaying with a 50% branching fraction to a top quark and the LSP or a bottom quark and the NLSP.
- **T2tt**: pair-produced top squarks, each decaying with a 100% branching fraction to a top quark and the LSP.

The corresponding Feynman diagrams are shown in Fig. 2.

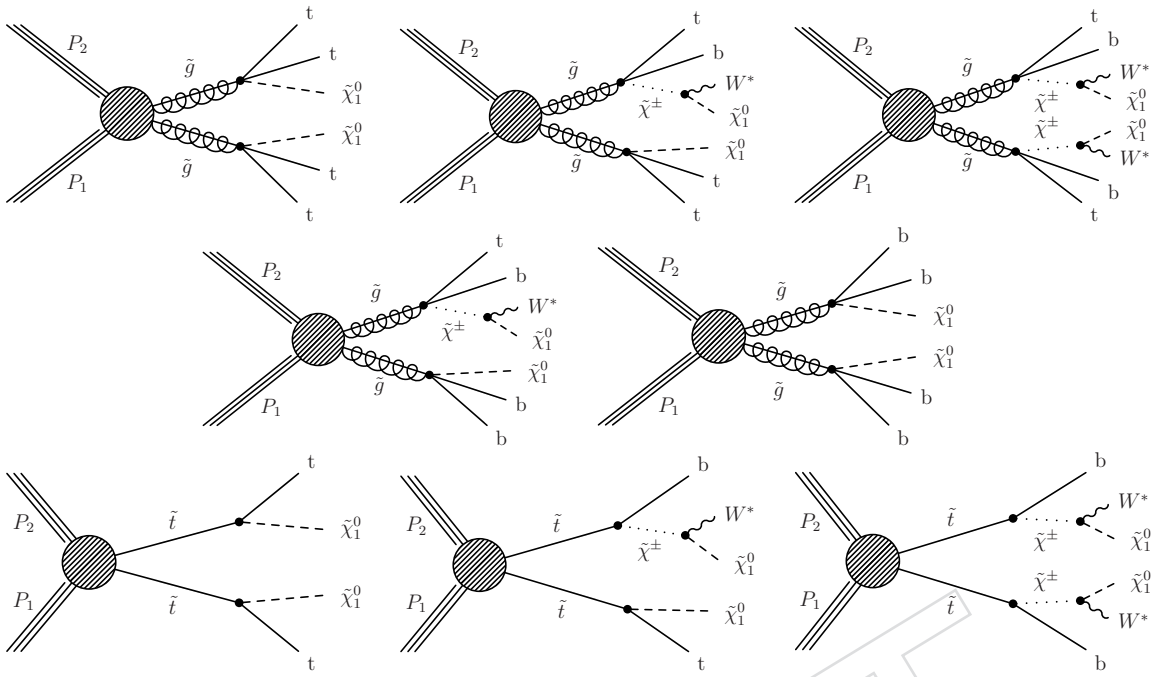

Figure 2: Diagrams displaying the event topologies of gluino (upper 5 diagrams) and top-squark (lower 3 diagrams) pair production considered in this paper.

We do not explicitly consider the corresponding simplified models for the bottom squark. Within the considered scenarios, a top-quark decay to a chargino (neutralino) is topologically similar to a bottom-squark decay to a neutralino (chargino). In the limit of degenerate charginos and neutralinos, the decay products of the chargino decay are generically too soft to be detected and this correspondence is exact. However, for large mass differences between the squarks and the chargino, the chargino decay products may be boosted enough to become observable, breaking the correspondence. With respect to the models without the intermediate decay to charginos, this implies a migration of reconstructed events from the low-background 2 b-Jet box to the high-background MultiJet box, and a consequently relatively weaker limit for the simplified model with decays to charginos. The exclusive single-lepton search is conservatively assumed to only have sensitivity when both top squarks decay to a top quark and a neutralino.

Events for the eight simplified models are generated with the MADGRAPH V5 simulation [35, 36], in association with up to two partons. The SUSY particle decays are treated with PYTHIA V6.4.26 assuming a constant matrix element (phase space decay). The event is showered in PYTHIA and matched to the matrix element kinematic configuration using the MLM algorithm [37], before being processed through a fast simulation of the CMS detector [38]. The SUSY particle production cross sections are calculated to next-to-leading order (NLO) and next-to-leading-logarithm (NLL) accuracy [39–43], assuming the decoupling of the other SUSY partners. The NLO+NLL cross section and the associated theoretical uncertainty [44] are taken as a reference to derive the exclusion limit on the SUSY particle masses.

3 The CMS detector

The central feature of the CMS detector [45] is a superconducting solenoid of 6 m internal diameter, providing a magnetic field of 3.8 T. Within the superconducting solenoid volume are

a silicon pixel and a silicon strip tracker, a lead tungstate crystal electromagnetic calorimeter (ECAL), and a brass/scintillator hadron calorimeter, each composed of a barrel and two endcap sections. Muons are measured in gas-ionization detectors embedded in the magnet steel flux-return yoke outside the solenoid. Extensive forward calorimetry complements the coverage provided by the barrel and endcap detectors. Events are detected by a two-level trigger system, based on a hardware filter (L1), followed by a software-based high level trigger (HLT).

The CMS experiment uses a coordinate system with the x-axis pointing towards the center of the LHC ring, the y-axis pointing up (perpendicular to the LHC plane), and the z-axis along the counterclockwise beam direction. The azimuthal angle ϕ is measured with respect to the x-axis in the xy plane and the polar angle θ is defined with respect to the z-axis. Pseudorapidity η is defined as $-\ln[\tan(\theta/2)]$. Jets and leptons are reconstructed within the region $|\eta| < 3$, covered by the ECAL and HCAL calorimeters. Muons are reconstructed with $|\eta| < 2.4$.

4 Event selection

The events are filtered at L1 requiring two jets in the central part of the detector. At the HLT, events are selected by dedicated HLT algorithms, consisting of a loose selection on M_R and R^2. The use of razor-specific triggers was chosen to preserve the shape of the SM background, which would be biased by a requirement on other traditionally used kinematic variables, e.g. E_T^{miss}. This is a necessary requirement, the background prediction is derived from a fit to a smooth function. The razor triggers reject the majority of the SM background at low R^2 and low M_R, while keeping the events in the signal-sensitive regions of the (M_R, R^2) plane. Two kinds of triggers are used: i) the hadronic razor trigger, selecting events with at least two jets having transverse momentum $p_T > 64\,\text{GeV}$ by applying threshold requirements on R^2, M_R, and their product; ii) the muon or electron razor triggers, combining looser requirements on R^2, M_R, and their product, with the requirement of at least one isolated muon or electron with $p_T > 12\,\text{GeV}$. The trigger efficiency, studied using a dedicated prescaled trigger, is measured to be $(95 \pm 5)\%$ and is independent of R^2 and M_R for the events selected by the baseline requirements described in Section 5.

After the offline event reconstruction, events are selected with at least one reconstructed interaction vertex. If more than one vertex is found, the one with the highest sum of p_T^2 of associated tracks is chosen as the interaction point for event reconstruction. Algorithms are used to remove events with detector- and beam-related noise that would mimic event topologies with high energy and large p_T imbalance [46, 47].

The analysis uses a global event description based on the CMS particle flow (PF) algorithm [48, 49]. Individual particles (PF candidates) are reconstructed by combining the information from the inner tracker, the calorimeters, and the muon system. Five categories of PF candidates are defined: muons, electrons, photons (including their conversions to e^+e^- pairs), charged hadrons, and neutral hadrons. The contamination from other proton-proton collisions in the same or in neighboring bunch crossings is reduced by discarding the charged PF candidates not compatible with the interaction point. When computing lepton isolation and jet energy, the corresponding contamination from neutral particles is subtracted on average by applying an event-by-event correction based on the jet-area method [50–52].

A "tight" lepton identification is used for muons and electrons, consisting of requirements on isolation and track reconstruction quality. For electrons, the shape and position of the energy deposit in the ECAL is used to further reduce the contamination from hadrons [53]. For events with one identified tight lepton, additional muons or electrons are identified through a "loose"

lepton selection, characterized by a relaxed isolation requirement [54]. In addition, tight leptons are required to have $p_T > 15$ GeV and loose leptons are required to have $p_T > 10$ GeV.

Jets are reconstructed by clustering the PF candidates with the FASTJET [55] implementation of the anti-k_T [56] algorithm with the distance parameter $R = 0.5$. We select events containing at least two jets with $p_T > 80$ GeV and $|\eta| < 2.4$, a tighter version of the L1 trigger criterion. The p_T imbalance in the event, $\vec{E}_T^{miss}$, is the negative of the sum of the $\vec{p}_T$ of the PF candidates in the event. For each event, the $\vec{E}_T^{miss}$ and the four-momenta of all the jets with $p_T > 40$ GeV and $|\eta| < 2.4$ are used to compute the razor variables, as described in Section 5.

The medium working point of the combined secondary vertex algorithm [57] is used for jet b tagging. The b-tagging efficiency and mistag probability are measured on data control samples, as a function of the jet p_T and η. Correction factors are derived for Monte Carlo (MC) simulations, comparing the b-tagging efficiency and mistag rate on multijet and $t\bar{t}$ data samples [57] to the corresponding values from simulation.

Events with no b-tagged jet are discarded, a criterion motivated by the expectation of a light top or bottom squark. A tighter requirement (≥ 2 b-tagged jets) is imposed on events without an identified tight lepton and fewer than four jets to reduce the $Z(\rightarrow \nu\bar{\nu})$+jets background to a negligible level.

5 Box definitions

The box definitions are given in Table 1. In the table, the boxes are listed according to the filling order, from the first (at the top of the table) to the last (at the bottom). If an event satisfies the requirements of two or more boxes, the event is assigned to the first listed box to ensure the boxes are disjoint samples.

The events in the single-lepton and two-lepton boxes are detected by the electron and muon razor triggers. The remaining two boxes, generically referred to as "hadronic" boxes, include events detected by the hadronic razor trigger.

In the two-lepton boxes, the (M_R, R^2) distribution of events with at least one b-tagged jet is studied. For the other boxes, the data are binned according to the b-tagged jet multiplicity: 1 b-tag, 2 b-tags, and ≥ 3 b-tags.

A baseline kinematic requirement is applied to define the region in which we search for a signal:

- $M_R > 400$ GeV and $R^2 > 0.25$ for the hadronic boxes,
- $M_R > 300$ GeV and $R^2 > 0.15$ for the other boxes.

The tighter baseline selection for the hadronic boxes is a consequence of the tighter threshold used for the hadronic razor trigger. The kinematic plane defined by the baseline selection is divided into three regions (see Fig. 3):

- **Low M_R sideband**: $400 < M_R < 550$ GeV and $R^2 > 0.30$ for the hadronic boxes; $300 < M_R < 450$ GeV and $R^2 > 0.20$ for the other boxes.
- **Low R^2 sideband**: $M_R > 450$ GeV and $0.25 < R^2 < 0.30$ for the hadronic boxes; $M_R > 350$ GeV and $0.15 < R^2 < 0.20$ for the other boxes.
- **Signal-sensitive region**: $M_R > 550$ GeV and $R^2 > 0.30$ for the hadronic boxes; $M_R > 450$ GeV and $R^2 > 0.20$ for the other boxes.

The bottom left corner of the razor plane, not included in any of the three regions, is excluded

Table 1: Kinematic and multiplicity requirements defining the nine razor boxes. Boxes are listed in order of event filling priority. The ranking is introduced to unambiguously associate an event to the first box it fills.

Requirements				
Box	Lepton	b-tag	Kinematic	Jet
Two-lepton boxes				
MuEle	$\geq$ 1 tight electron and $\geq$ 1 loose muon	$\geq$ 1 b-tag	($M_R > 300$ GeV and $R^2 > 0.15$) and ($M_R > 350$ GeV or $R^2 > 0.2$)	$\geq$ 2 jets
MuMu	$\geq$ 1 tight muon and $\geq$ 1 loose muon			
EleEle	$\geq$ 1 tight electron and $\geq$ 1 loose electron			
Single-lepton boxes				
MuMultiJet	1 tight muon	$\geq$ 1 b-tag	($M_R > 300$ GeV and $R^2 > 0.15$) and ($M_R > 350$ GeV or $R^2 > 0.2$)	$\geq$ 4 jets
EleMultiJet	1 tight electron			
MuJet	1 tight muon			2 or 3 jets
EleJet	1 tight electron			
Hadronic boxes				
MultiJet	none	$\geq$ 1 b-tag	($M_R > 400$ GeV and $R^2 > 0.25$) and ($M_R > 450$ GeV or $R^2 > 0.3$)	$\geq$ 4 jets
$\geq$ 2 b-tagged jet	none	$\geq$ 2 b-tag		2 or 3 jets

from the analysis. Given this selection, the multijet background from quantum chromodynamics processes is reduced to a negligible level due to the fact that these processes are typically balanced in the transverse plane and thus are peaking at zero in R^2 and exponentially suppressed above zero [30, 31].

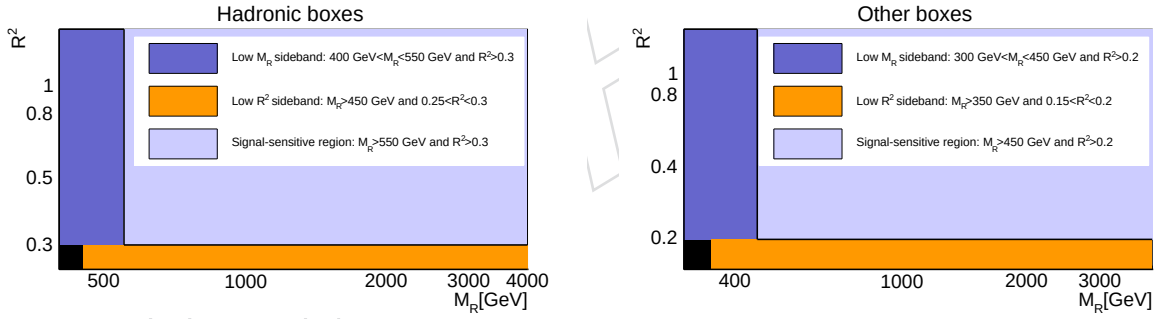

(a) (b)

Figure 3: Definition of the sideband and the signal-sensitive regions used in the analysis, for (a) the hadronic boxes and (b) the other boxes.

6 Modeling of the standard model backgrounds

Under the hypothesis of no contribution from new physics processes, the event distribution in the considered portion of the (M_R, R^2) plane can be described by the sum of the electroweak massive vector boson plus jets production (V+jets where V = W, Z) and the top quark-antiquark and the single top quark production, generically referred to as the $t\bar{t}$ contribution. Using Monte Carlo simulation, the contribution from other processes was verified to be negligible.

We study each of these processes using MC samples, generated with the MADGRAPH V5 simulation [35, 36]. Parton shower and hadronization effects are included by matching events to the PYTHIA V6.4.26 simulation [58] using the MLM algorithm [37]. The events are processed by a GEANT-based [59] description of the CMS apparatus to include detector effects.

Once normalized to the NLO inclusive cross section and the integrated luminosity, the absolute yield of the V+jets contribution satisfying the event selection is found to be negligible in all of the two-lepton boxes. In the remaining boxes, its contribution to the total SM background is found to be approximately 25%. The contribution of V+jets in the $\geq$ 2 b-tag and the $\geq$ 4 jet sample is found to be negligible. The rest of the background in each box originates from $\mathrm{t\bar{t}}$ events.

Based on the study of the data collected at $\sqrt{s} = 7$ TeV and the corresponding MC samples [30, 31], the two-dimensional probability density function $\mathrm{P_{SM}}(\mathrm{M_R}, \mathrm{R}^2)$ for each SM process is found to be well described by the empirical function:

$$f(\mathrm{M_R}, \mathrm{R}^2) = [b(\mathrm{M_R} - \mathrm{M_R^0})^{1/n}(\mathrm{R}^2 - \mathrm{R_0^2})^{1/n} - 1]e^{-bn(\mathrm{M_R}-\mathrm{M_R^0})^{1/n}(\mathrm{R}^2-\mathrm{R_0^2})^{1/n}}. \quad (4)$$

where b, n, $\mathrm{M_R^0}$, and $\mathrm{R_0^2}$ are free parameters of the background model. For $n = 1$, this function recovers the two-dimensional exponential function used for previous studies [30, 31]. The shape of the empirical function is determined through a ROOFIT-based extended and unbinned maximum likelihood fit to the data [60]. Two kinds of fits are performed: (i) a sideband-only fit, which is extrapolated to the signal region in order to test the presence of a signal (discussed in the remain of this section), and (ii) a simultaneous fit to the signal region and the sideband (both under the background-only hypothesis and the background-plus-signal hypothesis) for the interpretation of the result (see Sec. 7). In both cases, the empirical function is found to adequately describe the SM background in each of the boxes, for each b-tagged jet multiplicity.

The SM background-only likelihood function for the two-lepton boxes is written as:

$$\mathcal{L}(\mathrm{data}|\Theta) = \frac{e^{-\mathrm{N_{SM}}}}{\mathrm{N!}} \prod_{i=1}^{\mathrm{N}} \mathrm{N_{SM}} \mathrm{P_{SM}}(\mathrm{M_{R(}}_{i)}, \mathrm{R^2}_{(i)}) \,, \quad (5)$$

where $\mathrm{P_{SM}}(\mathrm{M_R}, \mathrm{R}^2)$ is the empirical function in Eq. (4) normalized to unity, N_{SM} is the corresponding event yield, Θ is the set of background shape and normalization parameters, and the product runs over the N events in that dataset. The same form of the likelihood is used for the other boxes, for each b-tagged jet multiplicity. The total likelihood in these boxes is computed as the product of the likelihood functions for each b-tagged jet multiplicity.

The fits are performed independently for each box and simultaneously across the b-tagged jet multiplicity bins. Common background shape parameters are used for the 2 b-tag and $\geq$ 3 b-tag bins, since no substantial difference between the two distributions is observed on large samples of $\mathrm{t\bar{t}}$ and V+jets MC events. A difference is observed between 1 b-tag and $\geq$ 2 b-tag samples, due to the observed dependence of the b-tagging efficiency on the jet p_{T}. Consequently, the shape parameters for the 1 b-tag bins are allowed to be different than the corresponding parameters for the $\geq$ 2 b-tag bins. The background normalization parameters for each b-tagged jet multiplicity bins are also treated as independent parameters.

The background shape parameters are estimated from the events in the two sidebands (see Section 5). This shape is then used to derive a background prediction in the signal-sensitive region: thousands of alternative background shape parameters are generated from the covariance matrix returned by the fit. An ensemble of pseudo-experiment datasets is created, generating random ($\mathrm{M_R}$, R^2) pairs distributed according to each of these alternative shapes. For each bin of

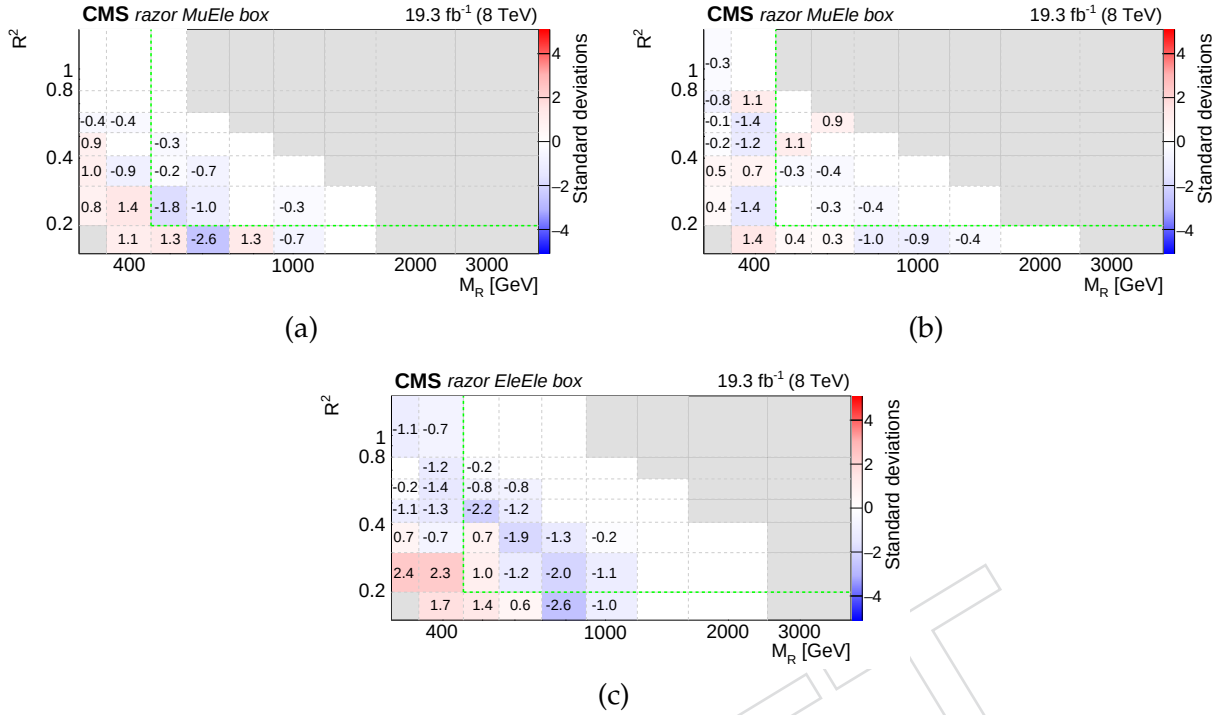

Figure 4: Comparison of the expected background and the observed yield in the (a) MuEle, (b) MuMu, and (c) EleEle boxes. A probability density function is derived for the bin-by-bin yield using pseudo-experiments, sampled from the output of the corresponding sideband fit. A two sided p-value is computed comparing the observed yield to the distribution of background yield from pseudo-experiments. The p-value is translated into the corresponding number of standard deviations, quoted in each bin and represented by the bin-filling color. Positive and negative significance correspond to regions where the observed yield is respectively larger and smaller than the predicted one. Gray areas correspond to empty bins with less than one background event expected on average.

the signal-sensitive region, the distribution of the predicted yields in each pseudo-experiment is compared to the observed yield in data in order to quantify the agreement between the background model and the observation. The agreement, quantified as a two-sided p-value, is then translated into the corresponding number of standard deviations for a normal distribution. The p-value is computed using the probability density as the ordering principle. The observed numbers of standard deviations in the two-lepton boxes are shown in Fig. 4, as a function of M_R and R^2. Positive and negative significance correspond to regions where the observed yield is respectively larger and smaller than the predicted one. Light gray areas correspond to empty bins with less than one event expected in average. Similar results for the one-lepton and hadronic boxes are shown in Figs. 5 and 6, respectively. Figures 7 to 10 illustrate the extrapolation of the fit results to the full (M_R, R^2) plane, projected on R^2 and M_R and summed over the b-tagged jet multiplicity bins. No significant deviation of data from the SM background predictions is observed.

To demonstrate the discovery potential of this analysis, we apply the background-prediction procedure to a simulated signal-plus-background MC sample. Figure 11 shows the M_R and R^2 distributions of the SM background events and of a sample of gluino-gluino production, with each gluino $\tilde{g}$ decaying to a $b\bar{b}$ pair and an LSP. The gluino and LSP masses are set respec-

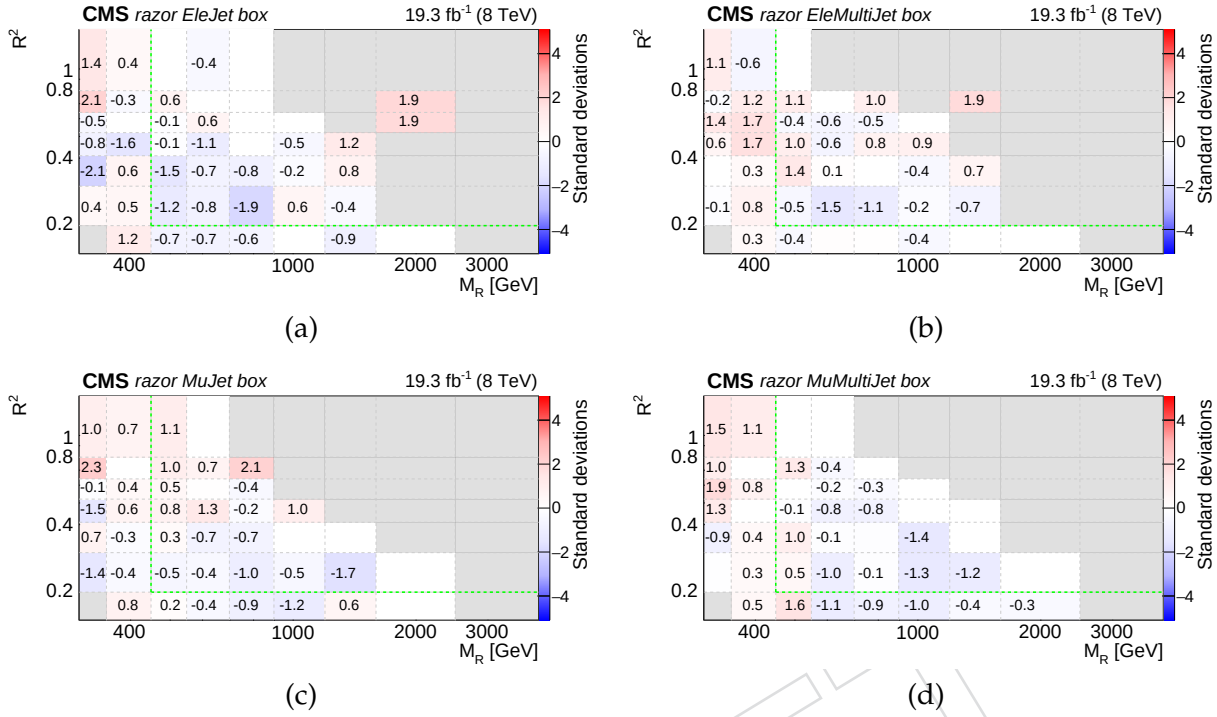

Figure 5: Comparison of the expected background and the observed yield in (a) the EleJet, (b) the EleMultiJet, (c) the MuJet, and (d) the MuMultiJet boxes. A detailed explanation is given in the caption of Fig. 4.

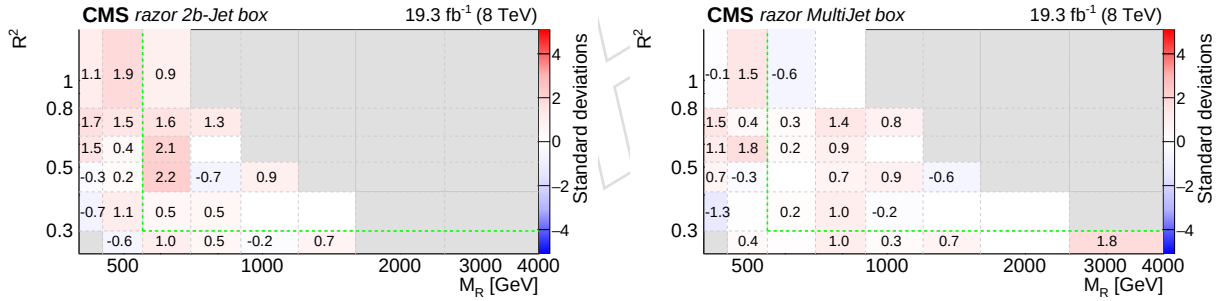

Figure 6: Comparison of the expected background and the observed yield in the 2 b-tagged jet box (left) and the MultiJet box (right). A detailed explanation is given in the caption of Fig. 4.

tively to 1325 GeV and 50 GeV, around the expected sensitivity of the search. A signal-plus-background sample is obtained adding the two distributions in Fig. 11, assuming an integrated luminosity of 19.3 fb^{-1} and a gluino-gluino production cross section of 0.02 pb, corresponding to 78 expected signal events in the signal-sensitive region. The agreement between the background prediction from the sideband fit and the yield of the signal-plus-background pseudo-experiments is displayed in Fig. 12. The signal contamination in the sideband has a negligible impact on the determination of the background shape, while a disagreement is observed in the signal-sensitive region, characterized as an excess of events clustered around $M_R \approx 1300$ GeV. The excess would indicate the presence of a signal, and the position of the excess along the M_R axis would provide information about the underlying SUSY spectrum.

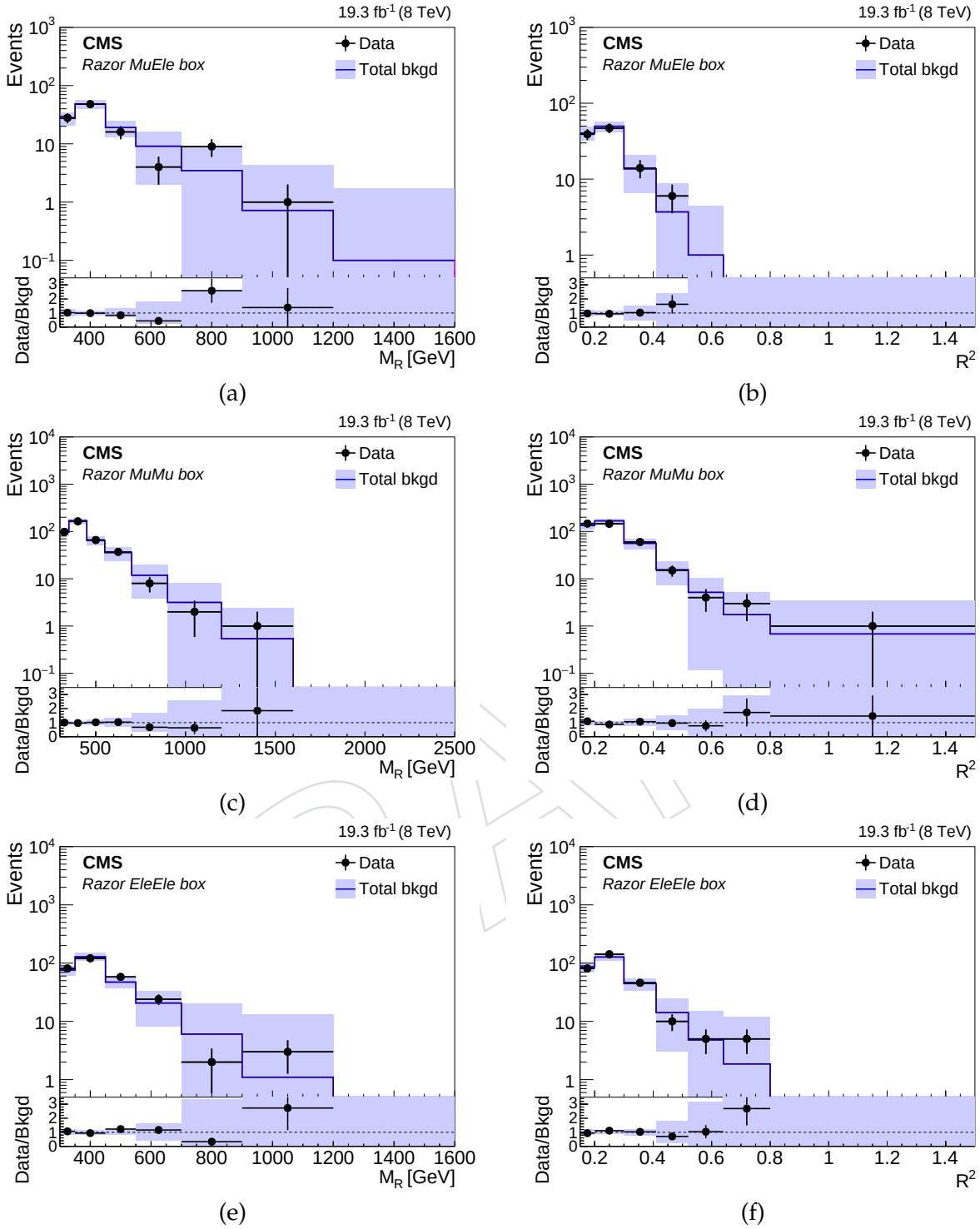

Figure 7: Projection of the sideband fit result in the (a-b) MuEle, (c-d) MuMu, and (e-f) EleEle boxes on M_R (left) and R^2 (right), respectively. The fit is performed in the sideband regions and extrapolated to the signal-sensitive region. The solid line and the filled band represent the total background prediction and its uncertainty. The points and the band in the bottom panel represent the data-to-prediction ratio and the prediction uncertainty, respectively.

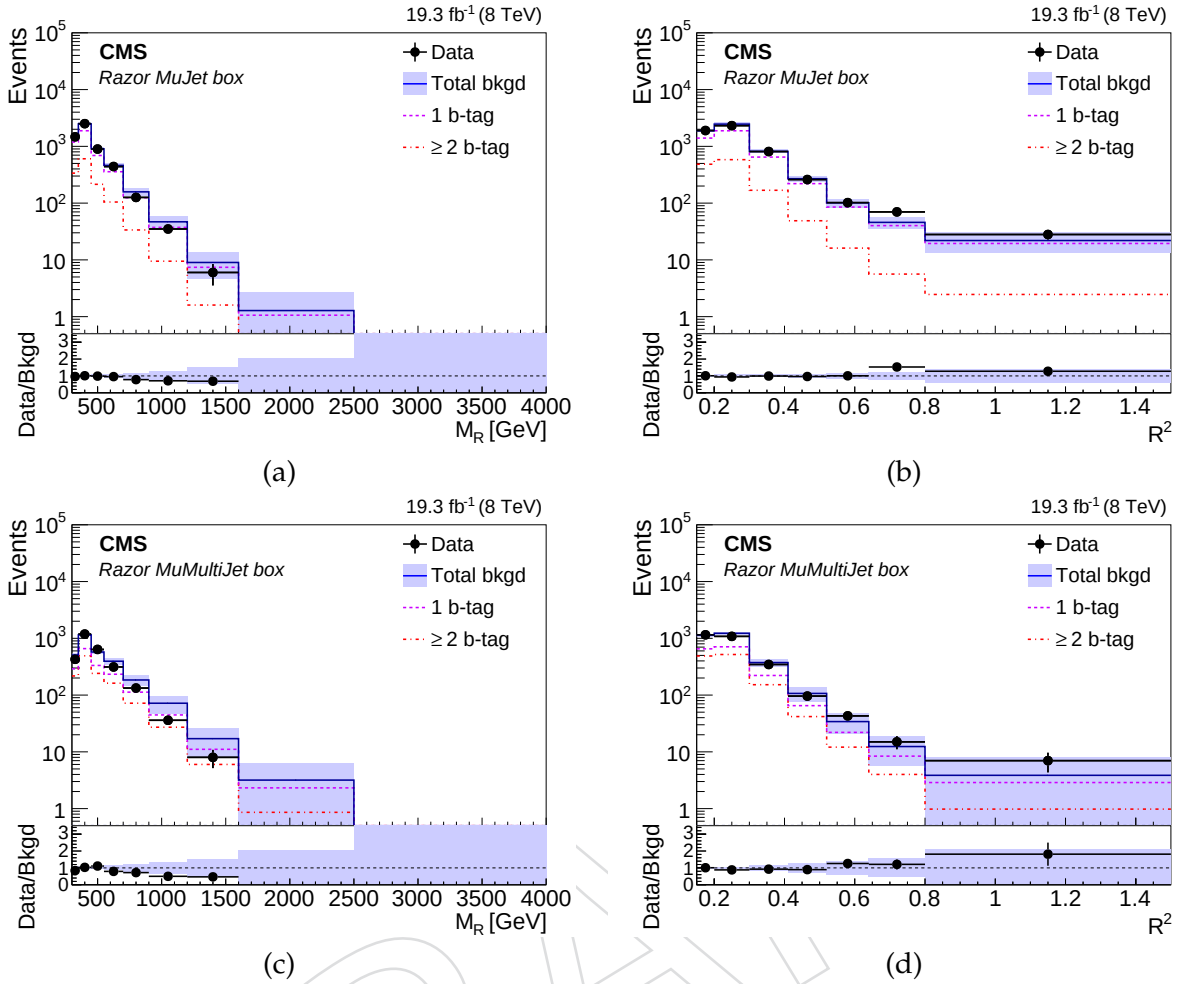

Figure 8: Projection of the sideband fit result in the MuJet box on (a) M_R and (b) R^2, and of the sideband fit result in the MuMultiJet box on (c) M_R and (d) R^2. The fit is performed in the sideband regions and extrapolated to the signal-sensitive region. The solid line and the filled band represent the total background prediction and its uncertainty. The dashed and dot-dashed lines represent the background shape for 1 b-tag and $\geq$ 2 b-tag events, respectively. The points and the band in the bottom panel represent the data-to-prediction ratio and the prediction uncertainty, respectively.

7 Limit setting procedure

We interpret the results of the searches by determining the 95% confidence level (CL) limit on SUSY models using the LHC CL_s procedure [32], combining the likelihoods of different search boxes in a global likelihood. In contrast to the procedure described in Section 6, a binned likelihood is used to speed up the computation of the exclusion limit on the SUSY particle masses, combining the sideband and the search region in a simultaneous fit. The 95% CL upper limit on the SUSY signal cross section (corresponding to the σ value at which $CL_s = 0.05$) is computed for each point of a given model's two-dimensional SUSY mass plane. The 95% CL mass exclusion contour is derived by intersecting this surface with the NLO+NLL cross section value surface.

For the razor search boxes, the signal contribution is modeled by a template function, for a given signal hypothesis in a specific box and a given b-tagged jet multiplicity. The template

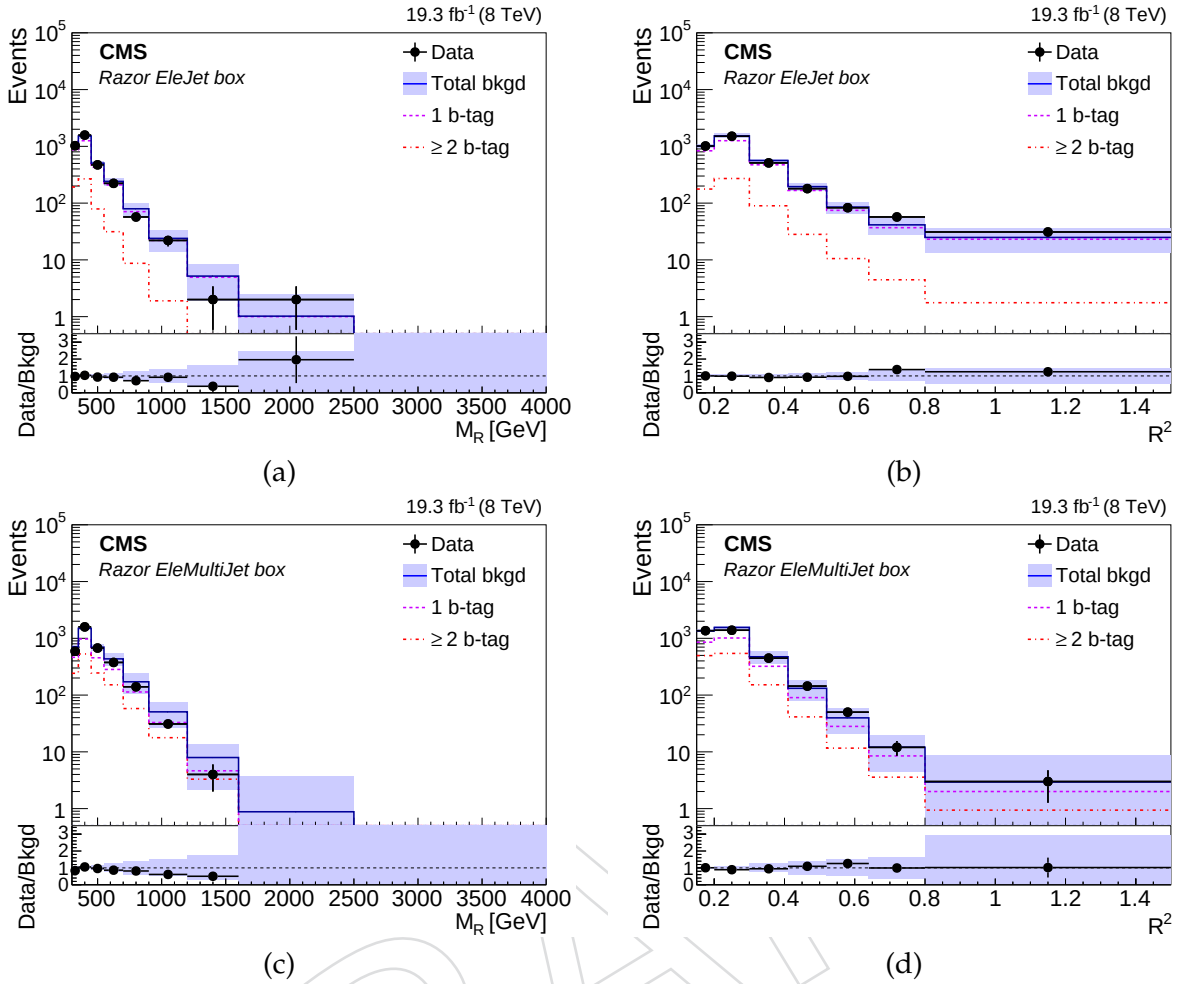

Figure 9: Projection of the sideband fit result in the EleJet box on (a) M_R and (b) R^2, and projection of the sideband fit result in the EleMultiJet box on (c) M_R and (d) R^2. A detailed explanation is given in the caption of Fig. 8.

function, normalized to unit probability, is multiplied by the expected signal yield in each bin ($\sigma \times L \times \epsilon^{\text{box}}_{\text{b-tag}}$). Here σ is the SUSY signal cross section, L is the integrated luminosity corresponding to the dataset size, and $\epsilon^{\text{box}}_{\text{b-tag}}$ is the signal selection efficiency for a given box and, in case of the single lepton and hadronic boxes, for a given b-tagged jet multiplicity.

Each systematic effect is incorporated in the likelihood with a dedicated nuisance parameter, whose value is not known a priori but rather must be estimated from the data. The additional flexibility in the parametric model introduced by each nuisance parameter results in a loss of sensitivity and adds an additional systematic uncertainty. The set of nuisance parameters may be divided into three distinct classes (though their statistical treatment is the same): those related to the signal normalization, those related to the signal shape, and those related to the background normalization and shape.

We consider the following systematic uncertainties associated with the signal normalization, the size of the uncertainty being indicated between parentheses for each of the categories stated below:

- integrated luminosity (2.6%) [61],

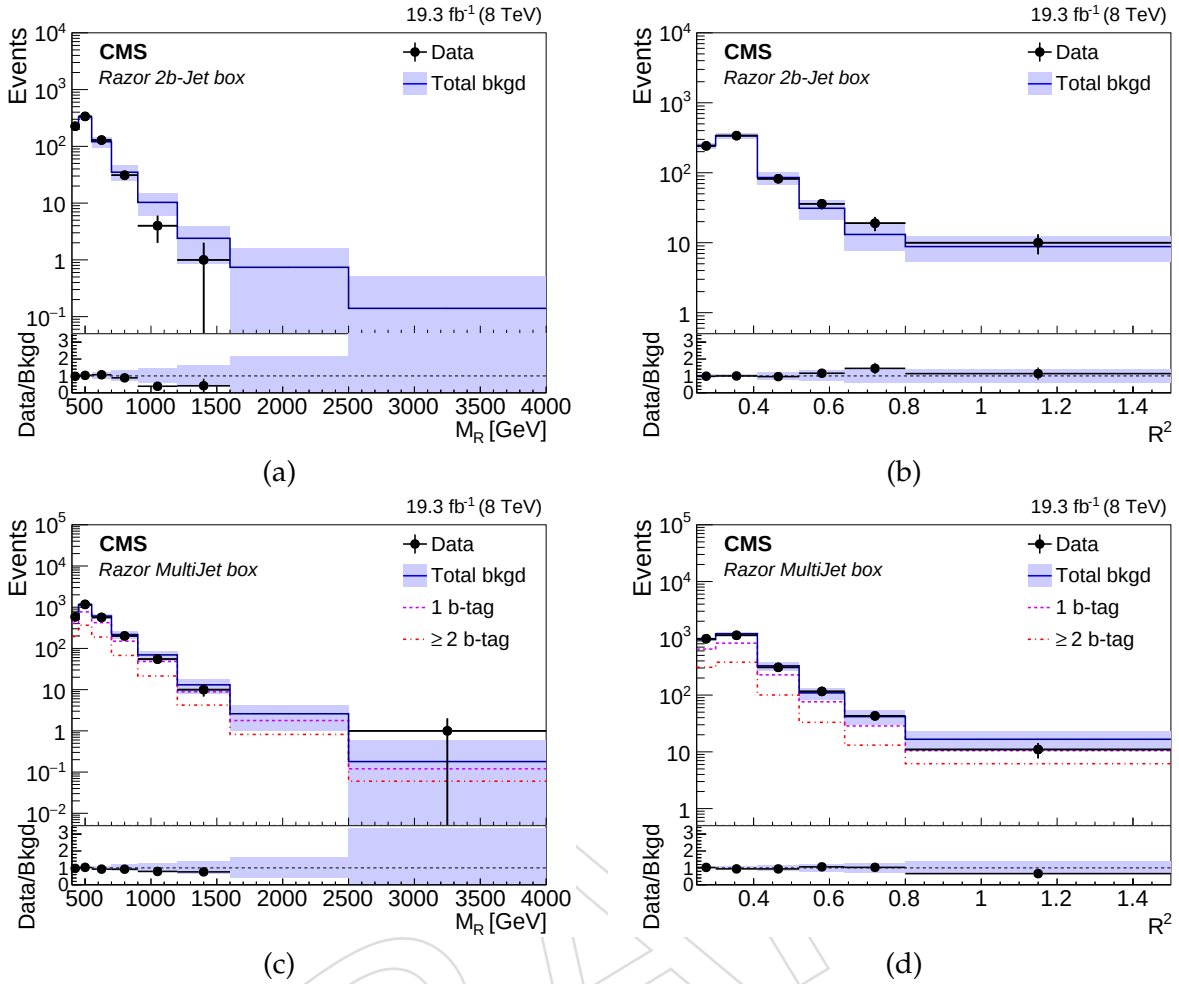

Figure 10: Projection of the sideband fit result in the 2 b-tagged jet box on (a) M_R and (b) R^2, and projection of the sideband fit result in the MultiJet box on (c) M_R and (d) R^2. A detailed explanation is given in the caption of Fig. 8.

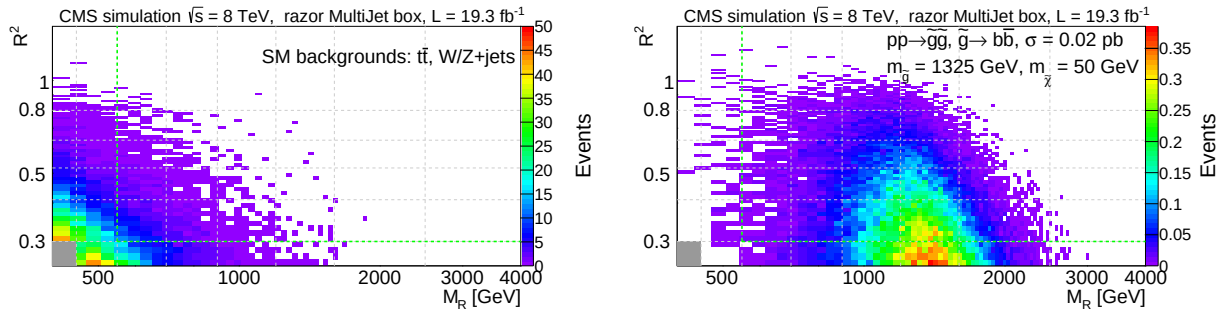

Figure 11: Distribution of (a) simulated SM background events and (b) gluino-gluino events in the MultiJet box. Each $\tilde{g}$ is forced to decay to a $b\bar{b}$ pair and a $\tilde{\chi}_1^0$, assumed to be the stable LSP. The $\tilde{g}$ and $\tilde{\chi}_1^0$ masses are fixed to 1325 GeV and 50 GeV, respectively.

- trigger efficiency (5%), and muon reconstruction and identification (3% per lepton), measured on an inclusive $Z \to \ell\ell$ sample as a function of the lepton p_T and η val-

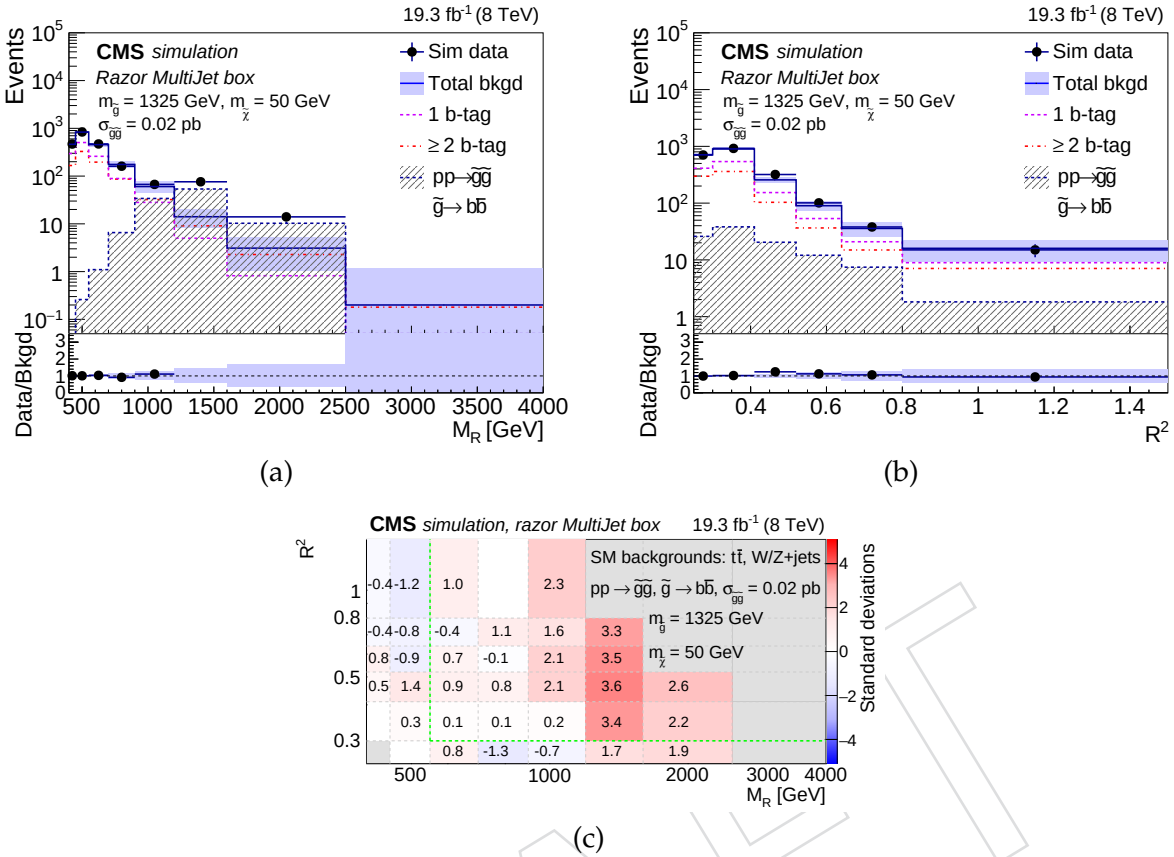

(a) (b) (c)

Figure 12: Result of the fit to the sideband events of a signal-plus-background MC sample, corresponding to the gluino model whose distribution is shown in Fig. 11. A gluino-gluino production cross section of 0.02 pb is assumed. The one-dimensional projections on (a) M_R and (b) R^2 are shown, together with (c) the agreement between the observed yield and the prediction from the sideband fit as a function of R^2 and M_R. This agreement is quantified by the two-sided p-value using an ensemble of background-only pseudo-experiment as described in Fig. 4.

ues [53, 54].

In addition, four signal shape systematic uncertainties are considered, whose sizes vary with R^2, M_R, and the b-tagged jet multiplicity:

- The uncertainty in the jet b-tagging and mistagging efficiencies (up to 20% depending on the particular signal), evaluated for each (M_R, R^2) and b-tagged jet multiplicity bin. The uncertainty is quantified by propagating the uncertainty in data-to-simulation scale factors [57],
- The uncertainty in the modeling of the parton distribution functions (PDFs) (up to 10% depending on the particular signal) evaluated bin-by-bin in the (M_R, R^2) plane for each box and b-tag multiplicity following the PDF4LHC prescription [62–64]. The report recommends the use of the predictions and the respective 68% CL uncertainty bands from different PDF sets to derive the final prediction (the mean of the different predictions) and the final uncertainty (the envelope of the different uncertainty bands) for the yield in one bin of a generic observable. In our study, `CTEQ-6.6` [65] and `MRST-2006-NNLO` [66] PDF sets were used.

- The uncertainty in the jet energy scale and resolution (up to 5% depending on the particular signal) evaluated from a set of data control samples and MC simulations [52],
- The uncertainty in the modeling of the associated jet production by the MADGRAPH simulation (up to 20% depending on the particular signal) studied on data samples of Z+jets and $t\bar{t}$, and parameterized by a MC-to-data scale factor as a function of the sum of the $\vec{p_T}$ of the two produced SUSY particles [14].

The impact of each of these uncertainties on the SUSY signal shape is taken into account by varying each effect up or down by one standard deviation to form the $\pm 1\sigma$ template distributions. Each effect is assigned a single nuisance parameter, which continuously interpolates between the nominal distribution and the $\pm 1\sigma$ template distributions.

The uncertainty in the knowledge of the background distributions is taken into account by maximizing the likelihood with respect to the background shape and normalization parameters using the data in the two sidebands and the signal-sensitive region. The background parameterization is able to accomodate several sources of systematic uncertainties defined below:

- dependence of the background shape on the b-tag multiplicity,
- dependence of the background shape on the lepton and jet multiplicities,
- deviation of the two-dimensional shape from an exponentially falling distribution, through the background empirical function parameter n, which modifies the tail in M_R and R^2,
- shape bias induced by the dependence of b-tagging efficiency and mistag rate on the jet p_T,
- deviation of the b-tagging and mistagging efficiencies from the MC prediction, through independent normalization factors in each b-tagged jet multiplicity bin.

The combination of razor and exclusive single-lepton searches is performed using the same procedure, taking into account the systematic uncertainties associated with the five following effects:

- the PDFs;
- the jet energy scale correction;
- the integrated luminosity;
- the b-jet tagging efficiency;
- the associated jet production.

The uncertainties in the background predictions are considered uncorrelated, being derived from independent data control samples with different techniques. We verified that the correlation model for the systematics has a negligible impact on the combination, since similar results are derived when neglecting any correlation between the systematic uncertainties of the two searches.

8 Interpretation

The result of this search is interpreted in the context of the natural SUSY simplified models of gluino-gluino and squark-squark production described in Section 2.

8.1 Limits on gluino pair production

Derived limits for gluino-gluino production decaying to top and bottom quarks are shown in Fig. 13. A comparison of the simplified natural SUSY gluino-gluino exclusions, obtained for the different decay-mode combinations of third generation quarks, is shown in Fig. 14. The limits corresponding to gluino-gluino topologies with mixed branching fractions lie within the band outlined by the T1bbbb and the T1tttt contours. As an example, gluino masses smaller than 1175 GeV for T1tttt and 1310 GeV for T1bbbb are excluded, depending on the gluino branching fractions, for an LSP mass of 100 GeV. For any LSP mass value, a larger number of top quarks in the decay topology corresponds to a weaker limit, mainly due to a reduced total signal efficiency with respect to the four-bottom-quark final state and a worse M_R and R^2 resolution for events with higher jet multiplicity in the final state. Given this fact and the inclusive nature of the analysis, the T1tttt limit can be considered a conservative estimate of a branching-fraction-independent limit, generically valid for gluino-gluino production within the context of the simplified SUSY spectrum shown in Fig. 1.

8.2 Limits on top-squark pair production

Derived limits for squark-squark production are shown for the search with razor variables in Fig. 15 and compared in Fig. 16, while those for the exclusive single-lepton top-squark search were reported previously [14]. Similarly, as in the case of the gluino interpretation, the expected limit from the razor search improves as the number of top quarks in the decay topology decreases. For an LSP mass of 100 GeV, top-squark mass values larger than 375 GeV and smaller than 660 GeV are excluded in all three top-squark branching fraction scenarios considered in the razor search.

A stronger limit on top-squark pair production is derived by combining the hadronic boxes of the razor search with the results of the exclusive single-lepton analysis. Figure 17 shows the combined result obtained for the scenario where the top squark only decays to a top quark and the lightest neutralino. For an LSP mass of 100 GeV, the combination improves the constraint on the top-squark mass from 660 to 730 GeV. This result provides the most stringent limit on these specific simplified models.

Figure 17 (c) shows a more generic limit on the top-squark mass. We consider two decay modes for the top squark, already introduced when discussing the simplified natural SUSY spectrum of Fig. 1 . We scan the relative branching fractions, assuming that no other decay mode is allowed. The largest excluded cross section (that is, the worst upper limit) is found for each top-squark and neutralino mass. A branching fraction independent limit is derived by comparing the worst-case exclusion to the corresponding top-squark pair production cross section. This way, top squarks decaying to the two considered decay modes are excluded at a 95% confidence level for mass values > 400 GeV and < 645 GeV, assuming a neutralino mass of 100 GeV. Unlike other simplified model interpretations, this interpretation is not based on a specific choice of branching fractions. While a residual model dependence is introduced when only two decay modes are considered, this result is more general than previous constraints.

9 Conclusion

We present a search for supersymmetric particles using proton-proton collision data collected by CMS at $\sqrt{s} = 8$ TeV. The dataset size corresponds to an integrated luminosity of 19.3 fb^{-1}. We consider events with at least two jets, at least one of which is identified as a b-tagged jet, and study the event distribution in the razor variables (M_R, R^2). The data are classified according to

the muon, electron, jet, and b-tagged jet multiplicities. No significant excess is observed over the SM background expectations, derived from a fit to the data distribution in low-M_R and low-R^2 sidebands.

The inclusive razor search is translated into a 95% confidence level exclusion limit on the masses of the gluino and the top squark, in the context of simplified "natural" SUSY models. For a neutralino mass of 100 GeV and depending on the branching fractions, the pair production of gluinos and top squarks in multi-bottom, multi-top, and mixed top-plus-bottom quark topologies is excluded for gluino masses up to 1310 GeV and top-squark masses up to 660 GeV. Using the combined likelihood of the hadronic boxes of the razor search and the single-lepton channels of the exclusive top-squark search, the exclusion bound on the top-squark mass is extended to 730 (640) GeV for a branching fraction $BR(\tilde{t} \to t\tilde{\chi}_1^0) = 100\%$ (50%) and for a neutralino mass of 100 GeV. For the same neutralino mass, top squarks decaying to the two considered decay modes are excluded at a 95% confidence level for mass values > 400 GeV and < 645 GeV, independent of branching fractions.

Acknowledgments

We congratulate our colleagues in the CERN accelerator departments for the excellent performance of the LHC and thank the technical and administrative staffs at CERN and at other CMS institutes for their contributions to the success of the CMS effort. In addition, we gratefully acknowledge the computing centres and personnel of the Worldwide LHC Computing Grid for delivering so effectively the computing infrastructure essential to our analyses. Finally, we acknowledge the enduring support for the construction and operation of the LHC and the CMS detector provided by the following funding agencies: BMWFW and FWF (Austria); FNRS and FWO (Belgium); CNPq, CAPES, FAPERJ, and FAPESP (Brazil); MES (Bulgaria); CERN; CAS, MoST, and NSFC (China); COLCIENCIAS (Colombia); MSES and CSF (Croatia); RPF (Cyprus); MoER, ERC IUT and ERDF (Estonia); Academy of Finland, MEC, and HIP (Finland); CEA and CNRS/IN2P3 (France); BMBF, DFG, and HGF (Germany); GSRT (Greece); OTKA and NIH (Hungary); DAE and DST (India); IPM (Iran); SFI (Ireland); INFN (Italy); NRF and WCU (Republic of Korea); LAS (Lithuania); MOE and UM (Malaysia); CINVESTAV, CONACYT, SEP, and UASLP-FAI (Mexico); MBIE (New Zealand); PAEC (Pakistan); MSHE and NSC (Poland); FCT (Portugal); JINR (Dubna); MON, RosAtom, RAS and RFBR (Russia); MESTD (Serbia); SEIDI and CPAN (Spain); Swiss Funding Agencies (Switzerland); MST (Taipei); ThEPCenter, IPST, STAR and NSTDA (Thailand); TUBITAK and TAEK (Turkey); NASU and SFFR (Ukraine); STFC (United Kingdom); DOE and NSF (USA).

Individuals have received support from the Marie-Curie programme and the European Research Council and EPLANET (European Union); the Leventis Foundation; the A. P. Sloan Foundation; the Alexander von Humboldt Foundation; the Belgian Federal Science Policy Office; the Fonds pour la Formation à la Recherche dans l'Industrie et dans l'Agriculture (FRIA-Belgium); the Agentschap voor Innovatie door Wetenschap en Technologie (IWT-Belgium); the Ministry of Education, Youth and Sports (MEYS) of the Czech Republic; the Council of Science and Industrial Research, India; the HOMING PLUS programme of Foundation for Polish Science, cofinanced from European Union, Regional Development Fund; the Compagnia di San Paolo (Torino); the Consorzio per la Fisica (Trieste); MIUR project 20108T4XTM (Italy); the Thalis and Aristeia programmes cofinanced by EU-ESF and the Greek NSRF; and the National Priorities Research Program by Qatar National Research Fund.

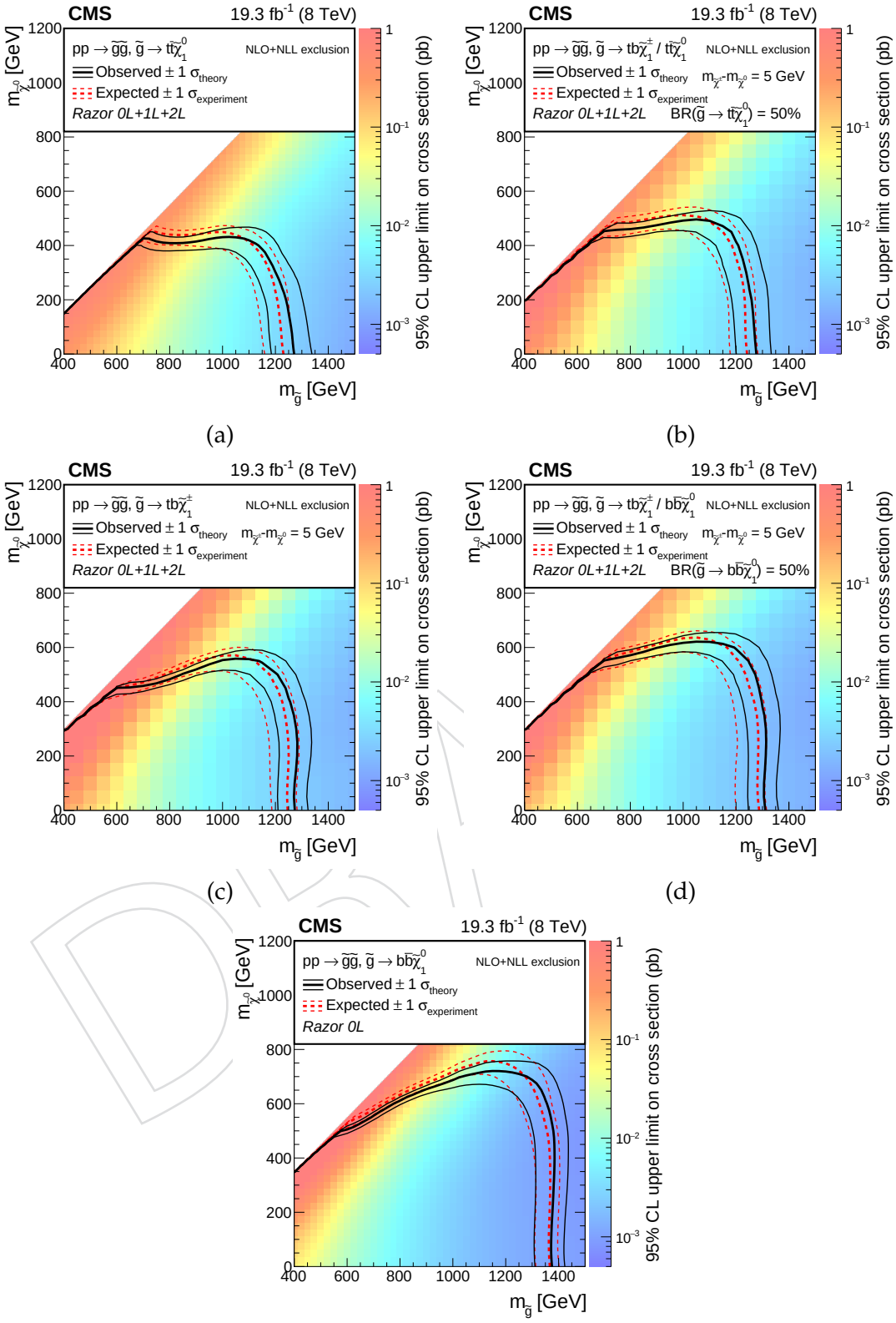

Figure 13: Interpretation of the inclusive search with razor variables in the context of gluino-mediated models: (a) T1tttt, (b) T1tttb, (c) T1ttbb, (d) T1tbbb, and (e) T1bbbb. The limit for T1bbbb is derived using only the hadronic boxes, while the limits for the remaining models are derived using all nine boxes. The color coding denotes the observed 95% CL upper limit on the signal cross section. The dashed and solid lines represent the expected and observed exclusion contours at a 95% CL, respectively. The dashed contours around the expected limit and the solid contours around the observed one represent the impact of the theoretical uncertainty in the cross section and the combination of the statistical and experimental systematic uncertainties, respectively.

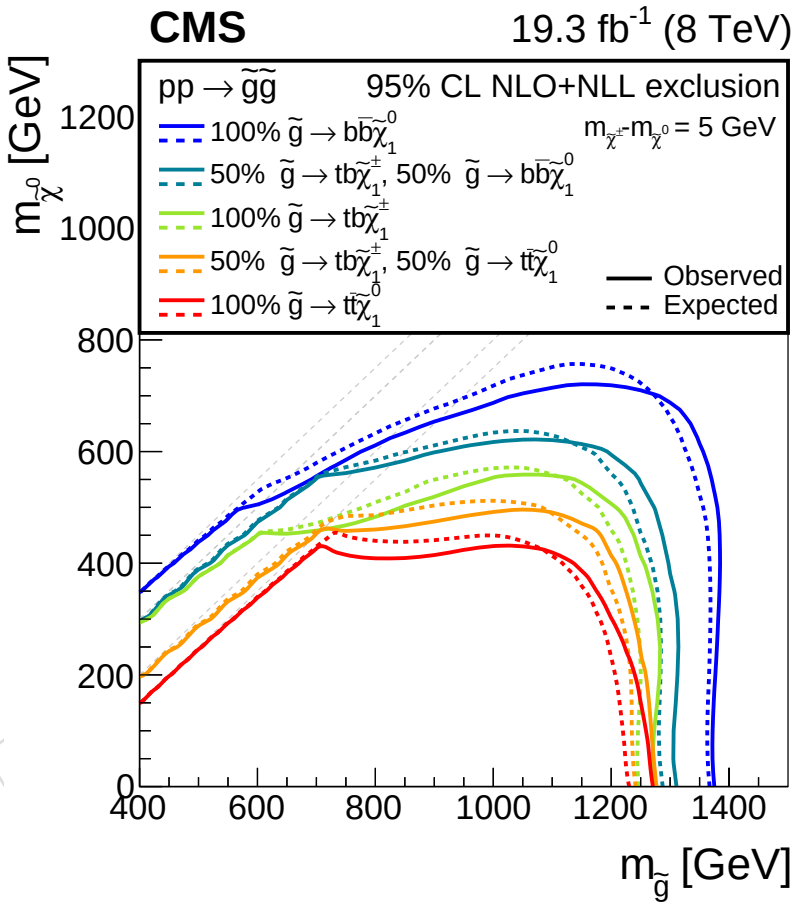

Figure 14: Gluino mass limit at a 95% CL, obtained for different gluino-gluino models with the inclusive razor analysis in the context of the benchmark natural SUSY spectrum of Fig. 1.

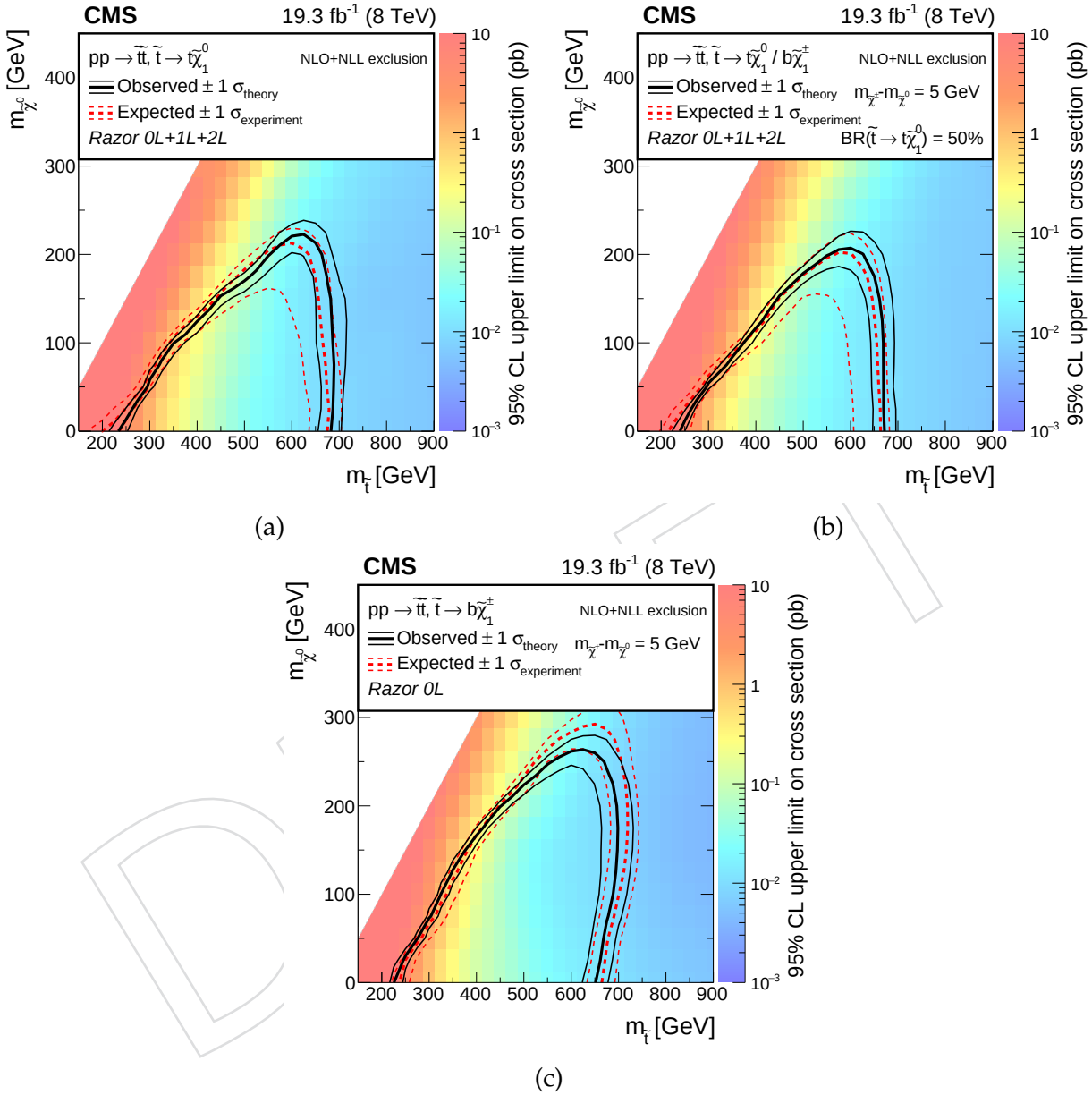

Figure 15: Interpretation of the inclusive search with razor variables in the context of top-squark-mediated models: (a) T2tt, (b) T2tb, and (c) T2bW*. The limit for T2bW* is derived using only the hadronic boxes, while the limits for the remaining models are derived using all nine boxes. The meaning of the color coding and the displayed contours are explained in the caption of Fig. 13.

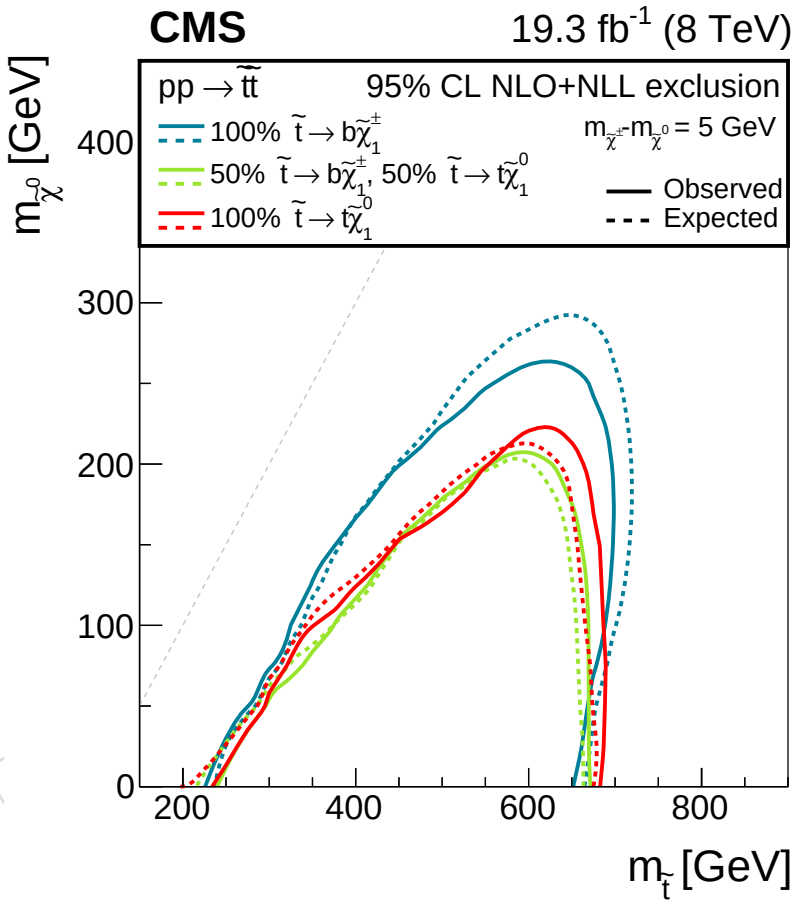

Figure 16: Top-squark mass limit at a 95% CL, obtained for different squark-squark models with the inclusive razor analysis in the context of the benchmark natural SUSY spectrum of Fig. 1.

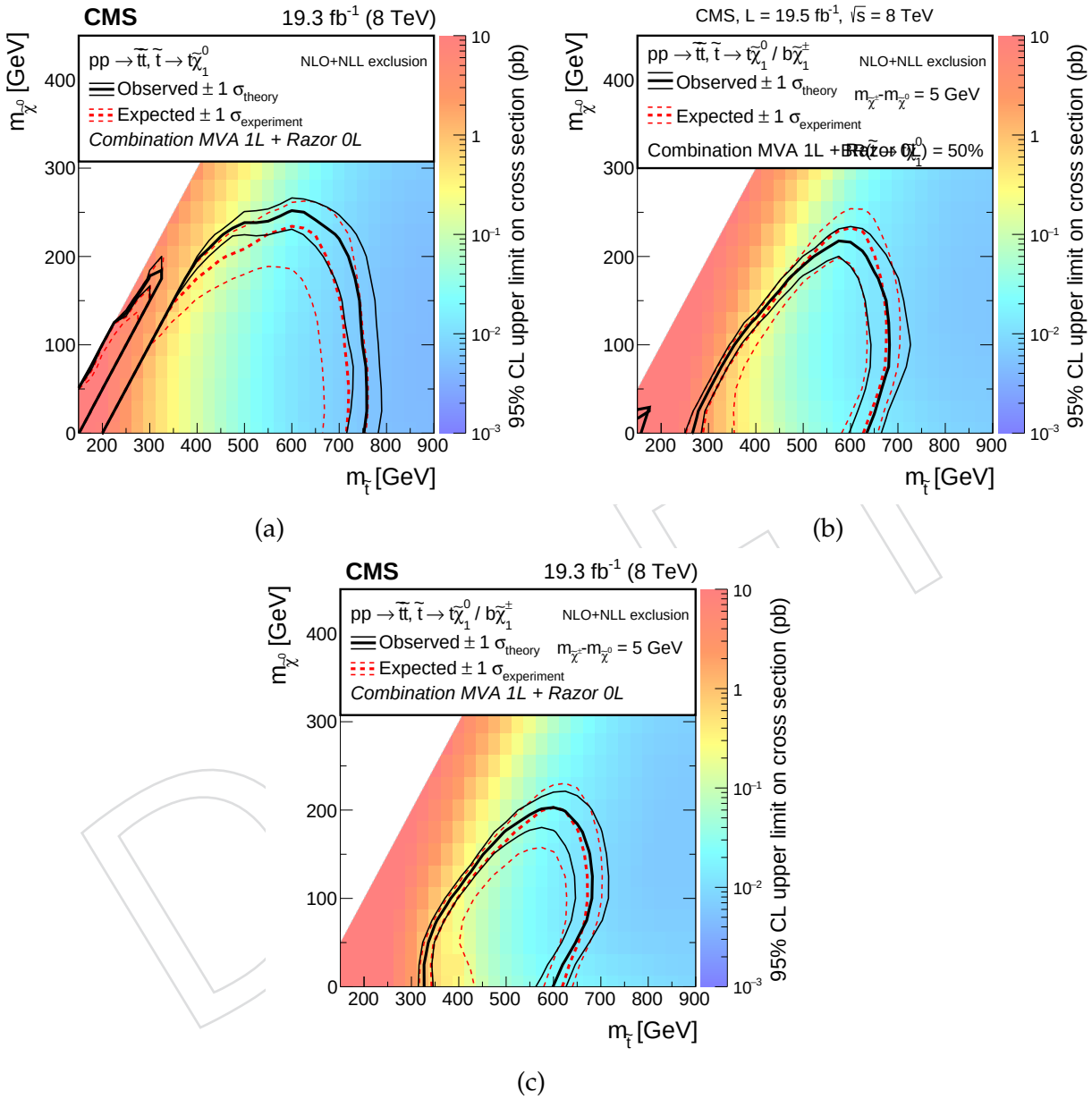

Figure 17: Top-squark mass limit at a 95% CL, obtained combining the result of the hadronic razor boxes with the result of Ref. [14] for (a) T2tt, (b) T2tb, and (c) independent of the branching fraction choice.

References

[1] J. Wess and B. Zumino, "Supergauge transformations in four-dimensions", *Nucl. Phys. B* **70** (1974) 39, doi:10.1016/0550-3213(74)90355-1.

[2] Y. A. Golfand and E. P. Likhtman, "Extension of the algebra of poincare group generators and violation of p invariance", *JETP Lett.* **13** (1971) 323.

[3] D. V. Volkov and V. P. Akulov, "Possible universal neutrino interaction", *JETP Lett.* **16** (1972) 438.

[4] A. H. Chamseddine, R. L. Arnowitt, and P. Nath, "Locally supersymmetric grand unification", *Phys. Rev. Lett.* **49** (1982) 970, doi:10.1103/PhysRevLett.49.970.

[5] G. L. Kane, C. F. Kolda, L. Roszkowski, and J. D. Wells, "Study of constrained minimal supersymmetry", *Phys. Rev. D* **49** (1994) 6173, doi:10.1103/PhysRevD.49.6173, arXiv:hep-ph/9312272.

[6] P. Fayet, "Supergauge invariant extension of the Higgs mechanism and a model for the electron and its neutrino", *Nucl. Phys. B* **90** (1975) 104, doi:10.1016/0550-3213(75)90636-7.

[7] R. Barbieri, S. Ferrara, and C. A. Savoy, "Gauge models with spontaneously broken local supersymmetry", *Phys. Lett. B* **119** (1982) 343, doi:10.1016/0370-2693(82)90685-2.

[8] L. J. Hall, J. D. Lykken, and S. Weinberg, "Supergravity as the messenger of supersymmetry breaking", *Phys. Rev. D* **27** (1983) 2359, doi:10.1103/PhysRevD.27.2359.

[9] P. Ramond, "Dual theory for free fermions", *Phys. Rev. D* **3** (1971) 2415, doi:10.1103/PhysRevD.3.2415.

[10] ATLAS Collaboration, "Observation of a new particle in the search for the Standard Model Higgs boson with the ATLAS detector at the LHC", *Phys. Lett. B* **716** (2012) 1, doi:10.1016/j.physletb.2012.08.020, arXiv:1207.7214.

[11] CMS Collaboration, "Observation of a new boson at a mass of 125 GeV with the CMS experiment at the LHC", *Phys. Lett. B* **716** (2012) 30, doi:10.1016/j.physletb.2012.08.021, arXiv:1207.7235.

[12] CMS Collaboration Collaboration, "Observation of a new boson with mass near 125 GeV in pp collisions at $\sqrt{s}$ = 7 and 8 TeV", *JHEP* **06** (2013) 081, doi:10.1007/JHEP06(2013)081, arXiv:1303.4571.

[13] M. Papucci, J. T. Ruderman, and A. Weiler, "Natural SUSY Endures", *JHEP* **09** (2012) 035, doi:10.1007/JHEP09(2012)035, arXiv:1110.6926.

[14] CMS Collaboration, "Search for top-squark pair production in the single-lepton final state in pp collisions at $\sqrt{s} = 8$ TeV", *Eur. Phys. J. C* **73** (2013) 2677, doi:10.1140/epjc/s10052-013-2677-2, arXiv:1308.1586.

[15] CMS Collaboration, "Search for new physics in the multijet and missing transverse momentum final state in proton-proton collisions at $\sqrt{s} = 8$ TeV", *JHEP* **06** (2014) 055, doi:10.1007/JHEP06(2014)055, arXiv:1402.4770.

[16] CMS Collaboration, "Search for supersymmetry in pp collisions at $\sqrt{s} = 8$ TeV in events with a single lepton, large jet multiplicity, and multiple b jets", *Phys. Lett. B* **733** (2014) 328, doi:10.1016/j.physletb.2014.04.023, arXiv:1311.4937.

[17] CMS Collaboration, "Search for new physics in events with same-sign dileptons and jets in pp collisions at $\sqrt{s} = 8$ TeV", *JHEP* **01** (2014) 163, doi:10.1007/JHEP01(2014)163, arXiv:1311.6736.

[18] ATLAS Collaboration, "Search for new phenomena in final states with large jet multiplicities and missing transverse momentum at $\sqrt{s} = 8$ TeV proton-proton collisions using the ATLAS experiment", *JHEP* **10** (2013) 130, doi:10.1007/JHEP10(2013)130, arXiv:1308.1841.

[19] ATLAS Collaboration, "Search for strong production of supersymmetric particles in final states with missing transverse momentum and at least three b-jets at $\sqrt{s} = 8$ TeV proton-proton collisions with the ATLAS detector", *JHEP* **10** (2014) 24, doi:10.1007/JHEP10(2014)024, arXiv:1407.0600.

[20] ATLAS Collaboration, "Search for supersymmetry at $\sqrt{s} = 8$ TeV in final states with jets and two same-sign leptons or three leptons with the ATLAS detector", *JHEP* **06** (2014) 035, doi:10.1007/JHEP06(2014)035, arXiv:1404.2500.

[21] ATLAS Collaboration, "Search for direct pair production of the top squark in all-hadronic final states in proton-proton collisions at $\sqrt{s} = 8$ TeV with the ATLAS detector", *JHEP* **09** (2014) 015, doi:10.1007/JHEP09(2014)015, arXiv:1406.1122.

[22] ATLAS Collaboration, "Search for direct top-squark pair production in final states with two leptons in pp collisions at $\sqrt{s} = 8$ TeV with the ATLAS detector", *JHEP* **06** (2014) 124, doi:10.1007/JHEP06(2014)124, arXiv:1403.4853.

[23] N. Arkani-Hamed et al., "MARMOSET: The path from LHC data to the new standard model via on-shell effective theories", (2007). arXiv:hep-ph/0703088.

[24] J. Alwall, P. Schuster, and N. Toro, "Simplified models for a first characterization of new physics at the LHC", *Phys. Rev. D* **79** (2009) 075020, doi:10.1103/PhysRevD.79.075020, arXiv:0810.3921.

[25] J. Alwall, M.-P. Le, M. Lisanti, and J. G. Wacker, "Model independent jets plus missing energy searches", *Phys. Rev. D* **79** (2009) 015005, doi:10.1103/PhysRevD.79.015005, arXiv:0809.3264.

[26] D. S. Alves, E. Izaguirre, and J. G. Wacker, "Where the sidewalk ends: jets and missing energy search strategies for the 7 TeV LHC", *JHEP* **10** (2011) 012, doi:10.1007/JHEP10(2011)012, arXiv:1102.5338.

[27] LHC New Physics Working Group Collaboration, "Simplified models for LHC new physics searches", *J. Phys. G* **39** (2012) 105005, doi:10.1088/0954-3899/39/10/105005, arXiv:1105.2838.

[28] C. Rogan, "Kinematics for new dynamics at the LHC", (2010). arXiv:1006.2727.

[29] CMS Collaboration, "Inclusive search for squarks and gluinos in pp collisions at $\sqrt{s} = 7$ TeV", *Phys. Rev. D* **85** (2012) 012004, doi:10.1103/PhysRevD.85.012004, arXiv:1107.1279.

[30] CMS Collaboration, "Inclusive search for supersymmetry using the razor variables in pp collisions at $\sqrt{s} = 7$ TeV", *Phys. Rev. Lett.* **111** (2013) 081802, doi:10.1103/PhysRevLett.111.081802, arXiv:1212.6961.

[31] CMS Collaboration, "Search for supersymmetry with razor variables in pp at $\sqrt{s}$=7 TeV", (2014). arXiv:1405.3961. CMS-SUS-12-005, CERN-PH-EP-2014-057, to appear in Phys. Rev. D.

[32] CMS and ATLAS Collaborations, "Procedure for the LHC Higgs boson search combination in Summer 2011", (2011). CMS-NOTE-2011-005.

[33] ATLAS Collaboration, "Multi-channel search for squarks and gluinos in $\sqrt{s} = 7$ TeV pp collisions with the ATLAS detector", *Eur.Phys.J. C* **73** (2013) 2362, doi:10.1140/epjc/s10052-013-2362-5, arXiv:1212.6149.

[34] CMS Collaboration, "Interpretation of Searches for Supersymmetry with Simplified Models", *Phys. Rev. D* **88** (2013) 052017, doi:10.1103/PhysRevD.88.052017, arXiv:1301.2175.

[35] J. Alwall et al., "MadGraph5: going beyond", *JHEP* **06** (2011) 128, doi:10.1007/JHEP06(2011)128, arXiv:1106.0522.

[36] J. Alwall et al., "The automated computation of tree-level and next-to-leading order differential cross sections, and their matching to parton shower simulations", *JHEP* **07** (2014) 079, doi:10.1007/JHEP07(2014)079, arXiv:1405.0301.

[37] S. Hoeche et al., "Matching parton showers and matrix elements", (2006). arXiv:hep-ph/0602031.

[38] CMS Collaboration, "The fast simulation of the CMS detector at LHC", *J. Phys. Conf. Ser.* **331** (2011) 032049, doi:10.1088/1742-6596/331/3/032049.

[39] W. Beenakker, R. Höpker, M. Spira, and P. M. Zerwas, "Squark and gluino production at hadron colliders", *Nucl. Phys. B* **492** (1997) 51, doi:10.1016/S0550-3213(97)80027-2, arXiv:hep-ph/9610490.

[40] A. Kulesza and L. Motyka, "Threshold resummation for squark-antisquark and gluino-pair production at the LHC", *Phys. Rev. Lett.* **102** (2009) 111802, doi:10.1103/PhysRevLett.102.111802, arXiv:0807.2405.

[41] A. Kulesza and L. Motyka, "Soft gluon resummation for the production of gluino-gluino and squark-antisquark pairs at the LHC", *Phys. Rev. D* **80** (2009) 095004, doi:10.1103/PhysRevD.80.095004, arXiv:0905.4749.

[42] W. Beenakker et al., "Soft-gluon resummation for squark and gluino hadroproduction", *JHEP* **12** (2009) 041, doi:10.1088/1126-6708/2009/12/041, arXiv:0909.4418.

[43] W. Beenakker et al., "Squark and gluino hadroproduction", *Int. J. Mod. Phys. A* **26** (2011) 2637, doi:10.1142/S0217751X11053560, arXiv:1105.1110.

[44] M. Krämer et al., "Supersymmetry production cross sections in pp collisions at $\sqrt{s} = 7$ TeV", (2012). arXiv:1206.2892.

[45] CMS Collaboration, "The CMS experiment at the CERN LHC", *JINST* **3** (2008) S08004, doi:10.1088/1748-0221/3/08/S08004.

[46] CMS Collaboration Collaboration, "Missing transverse energy performance of the CMS detector", *JINST* **6** (2011) P09001, doi:10.1088/1748-0221/6/09/P09001, arXiv:1106.5048.

[47] CMS Collaboration Collaboration, "Search for new physics in the multijet and missing transverse momentum final state in proton-proton collisions at $\sqrt{s} = 7$ TeV", *Phys. Rev. Lett.* **109** (2012) 171803, doi:10.1103/PhysRevLett.109.171803, arXiv:1207.1898.

[48] CMS Collaboration, "Particle–flow event reconstruction in CMS and performance for jets, taus, and $E_{\mathrm{T}}^{\mathrm{miss}}$", (2009). CMS-PFT-09-001.

[49] CMS Collaboration, "Commissioning of the particle-flow event reconstruction with the first LHC collisions recorded in the CMS detector", (2010). CMS-PFT-10-011.

[50] M. Cacciari, G. P. Salam, and G. Soyez, "The catchment area of jets", *JHEP* **04** (2008) 005, doi:10.1088/1126-6708/2008/04/005, arXiv:0802.1188.

[51] M. Cacciari and G. P. Salam, "Pileup subtraction using jet areas", *Phys. Lett. B* **659** (2008) 119, doi:10.1016/j.physletb.2007.09.077, arXiv:0707.1378.

[52] CMS Collaboration, "Determination of jet energy calibration and transverse momentum resolution in CMS", *JINST* **6** (2011) P11002, doi:10.1088/1748-0221/6/11/P11002, arXiv:1107.4277.

[53] CMS Collaboration, "Measurement of Higgs boson production and properties in the WW decay channel with leptonic final states", *JHEP* **01** (2014) 096, doi:10.1007/JHEP01(2014)096, arXiv:1312.1129.

[54] CMS Collaboration, "Measurement of the properties of a Higgs boson in the four-lepton final state", *Phys. Rev. D* **89** (2014) 092007, doi:10.1103/PhysRevD.89.092007, arXiv:1312.5353.

[55] M. Cacciari, G. P. Salam, and G. Soyez, "FastJet User Manual", *Eur. Phys. J. C* **72** (2012) 1896, doi:10.1140/epjc/s10052-012-1896-2, arXiv:1111.6097.

[56] M. Cacciari, G. P. Salam, and G. Soyez, "The anti-k_{T} jet clustering algorithm", *JHEP* **04** (2008) 063, doi:10.1088/1126-6708/2008/04/063, arXiv:0802.1189.

[57] CMS Collaboration, "Performance of b tagging at $\sqrt{s} = 8$ TeV in multijet, ttbar and boosted topology events", (2013). CMS-BTV-13-001.

[58] T. Sjöstrand, S. Mrenna, and P. Skands, "PYTHIA 6.4 physics and manual", *JHEP* **05** (2006) 026, doi:10.1088/1126-6708/2006/05/026, arXiv:hep-ph/0603175.

[59] GEANT4 Collaboration, "GEANT4: a simulation toolkit", *Nucl. Instrum. Meth. A* **506** (2003) 250, doi:10.1016/S0168-9002(03)01368-8.

[60] W. Verkerke and D. P. Kirkby, "The RooFit toolkit for data modeling", *eConf* **C0303241** (2003) MOLT007, arXiv:physics/0306116.

[61] CMS Collaboration, "CMS Luminosity Based on Pixel Cluster Counting - Summer 2013 Update", (2013). CMS-LUM-13-001.

[62] D. Bourilkov, R. C. Group, and M. R. Whalley, "LHAPDF: PDF use from the Tevatron to the LHC", (2006). arXiv:hep-ph/0605240.

[63] S. Alekhin et al., "The PDF4LHC Working Group Interim Report", (2011). arXiv:1101.0536.

[64] M. Botje et al., "The PDF4LHC Working Group Interim Recommendations", (2011). arXiv:1101.0538.

[65] P. M. Nadolsky et al., "Implications of CTEQ global analysis for collider observables", *Phys. Rev. D* **78** (2008) 013004, doi:10.1103/PhysRevD.78.013004, arXiv:0802.0007.

[66] A. Martin, W. Stirling, R. Thorne, and G. Watt, "Update of parton distributions at NNLO", *Phys. Lett. B* **652** (2007) 292, doi:10.1016/j.physletb.2007.07.040, arXiv:0706.0459.